Reduced SH3RF3 may protect against Alzheimer's disease by lowering microglial pro-inflammatory responses via modulation of JNK and NFkB signaling

Ronak Patel[1], Christopher L. Cardona[3], Ellen Angeles[1], Gunjandeep Singh[1], Archana Ashok[1], Andrew F. Teich[1,2,3], and Andrew A. Sproul[1,3,#]

[1]Taub Institute for Research on Alzheimer's Disease and the Aging Brain, Columbia University Irving Medical Center (CUIMC), New York, NY, USA.

[2]Department of Neurology, CUIMC, New York, NY, USA

[3]Department of Pathology and Cell Biology, CUIMC, New York, NY, USA

#Corresponding author and lead contact:

Andrew Sproul Ph.D. Email – aas2003@cumc.columbia.edu

Summary

Understanding how high-risk individuals are protected from Alzheimer's disease (AD) may illuminate potential therapeutic targets. A previously identified non-coding SNP in SH3RF3/POSH2 significantly delayed disease onset in a Caribbean Hispanic cohort carrying the PSEN1^{G206A} mutation sufficient to cause early-onset AD and microglial expression of SH3RF3 has been reported to be a key driver of late-onset AD. SH3RF3 acts as a JNK pathway scaffold and can activate NFκB signaling. While effects of SH3RF3 knockdown in human neurons were subtle, including decreased phospho-tau S422, knockdown in human microglia significantly reduced inflammatory cytokines in response to either a viral mimic or oligomeric Aβ42. This was associated with reduced activation of JNK and NFκB pathways in response to these stimuli. Pharmacological inhibition of JNK or NFκB signaling phenocopied SH3RF3 knockdown. We also found PSEN1^{G206A} microglia have reduced inflammatory responses to oAβ42. Thus, further reduction of microglial inflammatory responses in PSEN1 mutant carriers by protective SNPs in SH3RF3 might reduce the link between amyloid and neuroinflammation to subsequently delay the onset of AD.

Introduction

The amyloid hypothesis[1] has largely guided therapeutic approaches to treat Alzheimer's disease (AD) these past few decades. Although use of monoclonal antibodies to target Aβ removal has recently gained traction and FDA approval, clinical benefits are modest and carry risks such as ARIA-E (edema from blood brain barrier breakdown).[2,3] Additional therapeutic strategies are necessary. An alternative approach to targeting neuropathology directly is to better understand why some individuals are resilient to AD and then attempt to mimic this resistance via pharmacological manipulation or other interventions. One approach to better understand resilience is the study of genetic modifiers of the age of onset of AD in high-risk populations such as

presenilin-1 (PSEN1) mutation carriers, which is sufficient to cause early onset AD (EOAD). A non-coding SNP (rs6542814) in intron 1 SH3RF3/POSH2 (*plenty of SH3 domains 2*) was previously identified which delayed age of onset of AD by ~9.2 years in PSEN1 G206A carriers.[4] rs6542814 is associated with lower expression in fibroblasts in the Genotype-Tissue Expression Portal (GTEx) database (NES -0.19, p=1.69e-4). SH3RF3 has since been identified by causal interference analysis as a key microglial-expressed positive regulator of late-onset AD (LOAD) pathogenesis[5] and in a genome-wide association study (GWAS) focused on HIV-associated neurocognitive disorder (HAND).[6]

SH3RF3 functional domains include 4 protein-protein interaction SH3 domains, a novel Rac1 binding domain that only binds the active GTP-bound version, and a RING domain which gives SH3RF3 E3 ligase activity to target itself (and potentially other proteins) for proteasomal degradation. There are 3 SH3RF/POSH family members, which also include SH3RF1/POSH which has the same domain structure as SH3RF3, and SH3RF2/POSHER (*POSH-eliminating RING protein*), which is missing the 4th SH3 domain. Both SH3RF1 and SH3RF3 have been identified as scaffold proteins promoting JNK (c-Jun N-terminal kinase) signaling as well as having the ability to activate NFκB signaling by an unknown mechanism when overexpressed.[7-9] The ability to act as a JNK scaffold has best been described for SH3RF1,[10,11] which directly binds GTP-Rac1 and MAP3Ks such as MLK3 as well as JIP (*JNK-interacting protein*) family member scaffolds. JIP scaffolds in turn directly bind MAP2Ks (MKK4/7) and JNKs, which then phosphorylate c-Jun to activate the AP-1 transcription factor dimer (see also model **Figure 5**). On the other hand, SH3RF2/POSHER was reported to target SH3RF1/POSH for proteasomal degradation and interfere with its ability to promote JNK signaling.[12]

JNK and NFκB signaling pathways have both been shown to be strongly associated with AD pathogenesis and are activated by Aβ and upregulated in AD brains.[13-16] In neurons, JNK signaling has been shown to directly phosphorylate APP at T688 to promote amyloidogenic processing[17-19] and tau at multiple residues,[20,21] increase BACE1 transcription,[22] and is required for cell death of murine neurons from oligomeric Aβ42.[23] In microglia, JNK signaling has been reported to mediate Aβ-driven cytokine production[24], and has its activity increased by reduced TREM2 expression.[25,26] Interestingly, NFκB signaling has also been reported to drive BACE1 transcription and thus amyloidogenic processing.[27] The major pathogenic role of NFκB is that of a key driver of inflammatory responses such as production of pro-inflammatory cytokines and reactive oxygen species (ROS) in glial cells, which is both detrimental in itself to neurons and promotes amyloid and tau pathology as well as damage to the blood brain barrier.[15,16] Importantly, a recent study using human induced pluripotent stem cell (hiPSC)-derived microglia (iMGLs) xenotransplanted into an AD mouse model (APP^{NL-G-F}) demonstrated that human microglia have unique cytokine response modules (CRMs) in response to amyloid not seen in murine microglia.[28] CRMs are distinct from the DAM response by psuedotime analysis, are associated with NFκB signaling and pro-inflammatory cytokine production, and include SH3RF3 as a member (CRM2). Therefore, we postulated that reduced SH3RF3 expression or function would be protective against AD by mitigating extended activation of both JNK and NFκB pathways and tested this hypothesis in both hiPSC-derived neuronal and microglial (iMGLs) models.

Results

SH3RF3 knockdown does not affect APP processing in human neurons.

We first assessed loss of SH3RF3 function in human neurons produced by NGN2-mediated transdifferentiation of hPSCs (H9 hESC line) into excitatory neurons using a permanent line method developed by our lab (**Figure S1A**).[29] We used pooled siRNAs to knockdown (KD) SH3RF3 in neurons which was verified by qPCR (**Figure 1A**). We then tested for potential JNK pathway-related modulation of APP and Aβ production that might be modulated by SH3RF3 KD. In addition to the effects on APP processing described above for JNK signaling, APOE isoforms can differentially activate the AP1 transcription factor to increase APP transcription and Aβ production.[30] The downstream JNK target c-Jun can also activate AP1 when phosphorylated and dimerized with FOS. SH3RF3 KD resulted only in a trend of reduced APP transcription and total Aβ production (**Figure 1B-C**). Importantly, the Aβ42:Aβ40 ratio also remained unchanged (**Figure 1D**), and there was no effect on pAPP T688 (**Figure S1A**). This suggests that while protective SNPs in SH3RF3 may have subtle beneficial effects on modulating APP transcript levels, overall, it is unlikely that their protection against AD is primarily mediated through effects on Aβ production.

SH3RF3 knockdown decreases JNK-specific tau phosphorylation at ser422

We then assessed for effects of SH3RF3 KD on tau phosphorylation. We first confirmed SH3RF3 KD modulates JNK pathway activity in human neurons under basal and JNK pathway-inducing conditions. The protein phosphatase 2A inhibitor okadaic acid (OKA) activates JNK signaling in cultured hippocampal neurons and induces hyperphosphorylated tau and neuronal cell death.[31,32] OKA induced significant activation of JNK signaling in human neurons, which was moderately reduced by SH3RF3 KD (**Figure 1E**). S422 has been identified as a prominent JNK-induced phospho site in tau by mass spectrometry.[21] Tau S422 is expressed at very low levels under physiological conditions and co-localizes PHFs in AD brains,[33] and correlates with tangle formation in murine models of FTD and increased tau aggregation.[34,35] While pTau S422 was not detectable under basal conditions, SH3RF3 KD under OKA treatment conditions demonstrated a reduction in pTau s422 (**Figure 1F**). On the other hand, there was only a non-significant trend of decreased pTau T217, a potential blood marker of AD,[36,37] from SH3RF3 KD under OKA treatment conditions (**Figure S1B**). This suggests that protective SNPs that reduce SH3RF3 expression levels or function may modulate AD risk in part by affecting levels of phosphorylation levels of tau at specific phospho sites.

SH3RF3 KD reduces inflammatory cytokines produced by iMGLs treated with the viral mimic poly(I:C) by modulating JNK and NFκB signaling

We then tested if SH3RF3 KD had a more robust effect in microglia, where JNK and NFκB signaling have critical roles under pro-inflammatory conditions.[38,39] Further support from this approach came from looking at interactive published data sets of human and mouse CNS cells types, which showed that in the human brain SH3RF3 had its highest expression in microglia and fetal astrocytes (**Figure S2A;** brainrnaseq.org).[40]

Interestingly, this was not the case in the mouse brain, where expression was highest in neurons and low in microglia (**Figure S2B**),[41]suggesting species-specific differences in SH3RF3's functional role.

Multiple neurodegenerative diseases have shown strong associations with virus exposure. This includes AD, which is correlated with viral encephalitis, herpes simplex infections, HHV6, picornaviruses and HIV type 1.[42,43] Viral infections are postulated to increase Aβ production as a protective response leading to increased amyloid deposition and induction of inflammatory molecular pathways in the CNS.[44] This idea is supported by recent findings that show increase of Aβ in brains from subjects infected by COVID-19.[45,46] Various Pathogen Associated Molecular Patterns (PAMPs) can activate Toll-Like Receptors (TLRs) on the surface of microglia leading to microglial activation and release of inflammatory cytokines in response to microbes likes viruses and/or Aβ accumulation, which in turn cause neurotoxic damage.[47] Increased release of pro-inflammatory cytokines is also associated with damage to oligodendrocytes and BBB leakage, leading to exacerbation of AD pathology.[48,49] Inhibitors blocking microglial activation and release of inflammatory cytokines have been proposed as a potential AD therapeutic strategy.[50]

Thus, we utilized a viral mimic poly(I:C) to treat iMGLs, dsRNA known to elicit inflammatory microglial response via TLR3 activation.[51] iMGLs were differentiated from the FA0000010 (FA10) hiPSC line using a previously published protocol with minor modifications.[52] Most differentiated cells were $CD45^+/CD11B^+$ as measured by flow cytometry (**Figure S2C**) and expressed key microglial markers such as Iba1 and P2RY12 by immunostaining (**Figure S2D**). We used similar pooled non-targeting control siRNA and siRNA targeting SH3RF3 in iMGLs to knockdown SH3RF3 in presence and absence of poly(I:C) stimulation. We observed moderate knockdown of SH3RF3 by qPCR (**Figure 2A**). For assessing effects on pro-inflammatory cytokine production, we focused on 3 key Inflammatory cytokines, IL1β, IL6 and TNFα, which are also members of the human-specific CRM2 microglial cluster that appears in response to amyloid.[28] IL1β, IL6 and TNFα transcript levels upon 2h poly(I:C) stimulation showed strong upregulation compared to vehicle treated iMGLs, which were significantly reduced by SH3RF3 KD in poly(I:C) conditions. **(Figure 2B-D, Figure S2E).** This also translated to the protein level as measured by multiplex ELISA for IL1β, IL6 and TNFα from conditioned media from iMGLs at 16h post-treatment. Poly(I:C) treatment resulted in significantly higher release of IL1β, IL6 and TNFα which was significantly reduced by SH3RF3 KD **(Figure 2E-G).**

We then investigated whether modulation of JNK and NFκB signaling pathways were responsible for the SH3RF3 KD reduced inflammatory cytokine phenotype in iMGLs. SH3RF3 KD was performed in presence and absence of poly(I:C) treatment for 6 hours and lysates submitted for western blot. We observed increased JNK phosphorylation (Thr183 and Tyr185), and hence increased JNK activity, for multiple JNK isoforms upon poly(I:C) treatment **(Figure 2H).** SH3RF3 KD showed reduced JNK phosphorylation compared to control siRNA poly(I:C) treated conditions. We also assessed if poly(I:C) treatment of iMGLs could induce activation of the p65 (Rel-A) subunit of NF-kB signaling and the effect of SH3RF3 KD on NF-kB activation. We observed significantly upregulated p65 phosphorylation, demonstrating strong activation of NF-kB signaling, which also was reduced by SH3RF3 KD. (**Figure 2I**). Similar results were seen for the p105 subunit NFKB1 (**Figure S2F**). In summary,

148 SH3RF3 levels regulate activity of JNK and NF-kB signaling consistent with these pathways mediating
149 inflammatory response in iMGLs upon poly(I:C) stimulation.
150
151 **Pharmacological inhibitors of JNK and NF-kB phenocopy SH3RF3 KD**
152 To further solidify the mechanistic link between reduced JNK and NF-kB signaling and reduced cytokine
153 production in response to poly(I:C) treatment, we sought to determine if effects of SH3RF3 KD on inflammatory
154 cytokine production could be mimicked by pharmacological inhibition of these pathways. To inhibit JNK signaling,
155 we employed CEP-1347, a semisynthetic mixed lineage kinase (MLK) inhibitor, which blocks JNK activation by
156 inhibiting upstream MLK family member MAP3Ks.[53] CEP-1347 was used in a clinical trial for Parkinson's disease,
157 where it failed due to efficacy rather than safety concerns.[54] We also used IKK16, a selective inhibitor of IkB
158 kinase resulting in inhibition of canonical NF-kB signaling.[55] We treated iMGLs with poly(I:C) in presence of CEP-
159 1347, IKK16, or DMSO vehicle control and assessed inflammatory cytokine transcription. CEP-1347 and IKK16
160 produced significant reduction in transcription of all three inflammatory cytokines, although IKK16 was more
161 potent (**Figure 2J-L**). SH3RF3 interacts with activated RAC1 upstream to JNK and NF-kB kinases,[56] which led
162 us to hypothesize that inhibition of RAC1 activity might act similarly as SH3RF3 KD.[7] Treatment with the RAC
163 inhibitor NSC23766 also produced a similar phenotype as SH3RF3 KD with poly(I:C) stimulated iMGLs, although
164 used at a high concentration (50 μM) due to its low potency. (**Figure 21J-L**).[57] Taken together, this data
165 demonstrates that inhibition of JNK or NF-kB signaling is sufficient to lower inflammatory cytokine production in
166 iMGLs.
167
168 **SH3RF3 KD reduces inflammatory cytokines produced by iMGLs treated with oligomeric Aβ42 by**
169 **modulating JNK and NF-kB signaling**
170 We next wanted to extend our findings regarding effects of SH3RF3 KD on cytokine production to another
171 AD-relevant inflammatory stimuli. Oligomeric amyloidβ (oAβ) peptides are key drivers of AD according to the
172 amyloid hypothesis[1] and cause microglial activation and release of inflammatory cytokines.[58,59] We utilized a
173 commonly used Aβ oligomerization protocol[60] which we then assessed for oligomerization state. Coomassie blue
174 staining for total protein showed one dominant band consistent with Aβ trimers and no high order species (**Figure**
175 **3A**). Interestingly, western blot using the 6E10 Aβ antibody showed the presence of higher order oligomers
176 (**Figure 3B**), which presumably have greater affinity for the antibody by having multiple epitopes even though a
177 minority product. oAβ42 treatment of iMGLs for 24h resulted in induction of inflammatory cytokines as assessed
178 by qPCR for IL1β, IL6 and TNFα transcripts compared to vehicle treated controls (**Figure 3C-E**). Corroborating
179 with our previous results with poly(I:C) stimulated iMGLs, SH3RF3 KD produced significantly reduced transcripts
180 for all 3 cytokines.
181 Although we initially started with 24h treatment as a point of analysis, we realized that oAβ42 would also
182 be actively phagocytosed by iMGLs which would reduce the potency of the stimulus over time. We hypothesized
183 this could at least partially explain a recently published study which only showed minor transcriptional effects of
184 iMGLs treated for 24 hours with oAβ42,[61] although that study also used a lower concentration of oAβ42 (1μM

instead of 5μM) and potentially had a different Aβ oligomerization state. Thus, we did a time course experiment, which showed transcriptional responses at 24h to oAβ42 were already much lower than at earlier 6h and 12h time points (**Figure S3A**). We also determined that NF-kB signaling was activated by 3h as assessed by western blot and was more robust for 5μM as compared to 1μM oAβ42 (**Figure S3B**).

Upon learning that oAβ42 transcriptional effects were blunted by 24h post-treatment, we tested if iMGLs treated with oAβ42 for 3h released inflammatory cytokines and if SH3RF3 KD affected this response. While IL1β levels were not increased by oAβ42 at this time point, IL6 and TNFα levels were significantly elevated (**Figure 3F-G**). SH3RF3 KD significantly reduced TNFα release and trended towards reducing IL-6. We also evaluated effects of oAβ42 on JNK and NF-kB pathways in the presence of SH3RF3 KD. As anticipated, oAβ42 activated JNK and NF-kB pathways as observed by increased phosphorylation of JNK and p65. (**Figure 4A-B**) as well as p105 (**Figure S4A**). Similar to poly(I:C) treatment, SH3RF3 KD reduced activation of JNK and NF-kB signaling. We also performed similar chemical inhibitor experiments which demonstrated that JNK inhibition by CEP-1347 or NF-kB by IKK16, were sufficient to block inflammatory cytokine production by oAβ42 in iMGLs (**Figure 4C-E**). In summary, inflammatory cytokines produced by iMGLs treated with oAβ42 are also attenuated by SH3RF3 KD, which is likely mediated by reduced activation of JNK and NF-kB signaling.

PSEN1^{G206A} microglia have reduced induction of cytokines in response to oligomeric Aβ42

We hypothesized that SH3RF3 protective SNPs might be particularly beneficial in a PSEN1 mutant background. It has been previously reported that PSEN1$^{\Delta E9}$ iMGLs have reduced inflammatory responses to bacterial lipopolysaccharide (LPS) relative to isogenic control iMGLs.[62] To test if PSEN^{G206A} iMGLs also reduced inflammatory responses, we knocked the G206A mutation into both alleles of PSEN1 in the IMR90 (cl.4) hiPSC line using CRISPR/Cas9 (**Figure S4B**). Homozygous rather than hemizygous knock-in was confirmed via qgPCR (data not shown).[63] PSEN1^{G206A} and isogenic control iMGLs were then treated with oAβ42 for 6h to look for transcriptional effects on IL1β, IL6 and TNFα (**Figure 4F**). While the level of transcriptional response to oAβ42 were more variable between independent experiments using these lines, IL1β and IL6 were consistently reduced in PSEN1^{G206A} iMGLs compared to isogenic control iMGLs. TNFα trended lower. This suggests that microglia in subjects with PSEN1 mutations may have reduced pro-inflammatory responses in general.

Discussion

It is critical to understand the mechanisms of why some high-risk individuals are protected from getting AD as an alternative therapeutic strategy to targeting neuropathological changes in amyloid and tau directly. Thus, we sought to understand the mechanisms of how a protective SNP in SH3RF3[4] delayed onset of AD in PSEN^{G206A} carriers. We focused on JNK and NF-kB signaling since SH3RF family members including SH3RF3 had been shown to be able to activate these pathways.[7-10] For JNK signaling, SH3RF proteins (as best described for SH3RF1/POSH) act as scaffolds linking upper and lower components of this MAPK cascade.[10,11] The mechanism(s) of how SH3RF3 modulates NF-kB activity is not well understood and should be the subject of further research. We initially focused on neurons, as early-onset AD mutations like those in PSEN1 are primarily

222 thought to drive disease through modulating APP processing, such as by increased Aβ42:Aβ40 ratio. However,
223 SH3RF3 KD did not affect APP processing in a significant fashion under steady-state conditions (**Figure 1**).
224 SH3RF3 KD did decrease phosphorylation at the JNK-specific tau S422 phospho-site which could have some
225 effect on AD risk. It is important to note that while phosphorylation of the S422 site of tau is found in PHFs in AD
226 brains[33] and has been proposed to be pathogenic,[64] it also been reported that phosphorylation of tau at S422
227 blocks caspase 3 cleavage of tau,[65] which is considered a pro-pathogenic event. In addition, one significant
228 caveat of our neuronal studies is that as JNK and NF-kB are stress-induced signaling cascades, thus, SH3RF3
229 may play a stronger role in neurons in response to specific stresses not tested here.

230 We then chose to look at microglia as JNK and NF-kB signaling are also critical for inflammatory
231 responses in this cell type.[38,39] We chose to focus our analysis on 3 pro-inflammatory cytokines, IL1β, IL6 and
232 TNFα, which have been associated with AD and are members of a human-specific microglial cytokine response
233 cluster (CRM2) activated in human microglia xenotransplanted into the APP^{NL-G-F} AD mouse model.[28] SH3RF3
234 KD, mimicking protective a SNP[4] that lower its expression, can blunt pro-inflammatory cytokine production from
235 two AD-relevant stresses, a viral mimic poly(I:C) and oAβ42 (**Figures 2-4**). This was associated with reduced
236 JNK and NF-kB signaling, and blockade of these pathways through chemical inhibitors was sufficient to reduce
237 inflammatory cytokine production. Overall, our data is consistent with a model where reduced expression of
238 SH3RF3 by protective SNPs lowers inflammatory cytokines produced by inflammatory insults by dampening
239 JNK and NF-kB signaling, to consequently delay the onset of AD (**Figure 5**). Interestingly, while genes expressed
240 primarily in microglia have almost exclusively been associated with late-onset forms of AD, and early-onset AD
241 has been associated with neuronal acting genes, our study suggests that early-onset AD risk may also be
242 significantly influenced by genetic modulators of microglial function.

243 One limitation of our study is that we focused exclusively in microglia on inflammatory cytokine
244 production. Other inflammatory responses such as ROS production or effects on phagocytosis should be
245 addressed in future studies. Regarding inflammatory reaction of iMGLs oAβ42, it is important to note that this is
246 a very transient response that could reflect elevated oAβ from transient pathological events like ischemia which
247 increase Aβ levels,[66] rather than a more "DAM"-like response to aggregated fibrillar forms of Aβ. On the other
248 hand, xenotransplantation of iMGLs into the APP^{NL-G-F} AD mouse model[28] had human-specific cytokine modules
249 under both steady-state responses to amyloid and co-injection of oAβ42, suggesting a broader role of
250 inflammatory cytokine production in the human microglial response to AD pathology. Importantly, SH3RF3 was
251 a member of the CRM2 module suggesting it could help drive this cluster which could be tested in future
252 xenotransplantation experiments.

253 Finally, a key goal of trying to understand the molecular mechanisms of AD protective SNPs was to mimic
254 those genetic protective mechanisms with small molecules. We found CEP-1347, a MAP3K inhibitor that blocks
255 JNK signaling,[53] significantly reduced inflammatory cytokine production in iMGLs from both a viral mimic and
256 oAβ42. CEP-1347 and other MAP3K inhibitors have previously shown benefits in blunting inflammatory
257 responses in other microglial/macrophage models and promote Aβ clearance.[24,67,68] Importantly, CEP-1347 has
258 also been shown to block neuronal cell death from oAβ42, trophic factor withdrawal, UV, and oxidative stress.[23,69]

This data led, at least in part, to CEP-1347 being tested in the PRECEPT trial for Parkinson's disease (PD), where it failed for efficacy rather than safety concerns.[70] One possible reason for this failure was that cell death in PD has been reported to be driven by the MAP3K DLK[71], which CEP-1347 inhibits to a much lesser degree than MLKs.[53] In addition, genetic evidence suggests that microglia play a more dominant role in AD than PD, and therefore, CEP-1347 effects on microglial inflammatory responses would be expected to have greater importance in AD. Thus, reconsideration of using MAP3K (MLK) inhibitors like CEP-1347 to treat AD may be warranted as this could act as a double hit to both dampen pro-inflammatory microglial responses and to protect neurons from cell death from Aβ and other insults. This particularly could be the case for PSEN1 mutant carriers, as we (**Figure 4F**) and others[62] have seen a lower baseline inflammatory response in PSEN1 mutant microglia, as well as PSEN1 mutant carriers having a more clearly amyloid-driven form of AD.

Acknowledgements

This work was supported by R01AG058918-05 (AAS Co-I), 1P30AG066462-01 (A.A.S. Co-PI on Development Grant), the Henry and Marilyn Taub Foundation (A.A.S.), and TAME-AD (Thompson Foundation, A.A.S.). We would also like to thank Sabrina Miller (East Side Community School) for experiments during her summer research internship (Columbia University Summer Research Program for Science Teachers) verifying SH3RF3 acted as a JNK pathway scaffold as previously reported.

Keywords

Alzheimer's disease, PSEN1, SH3RF3, POSH2, JNK, NFκB, Microglia, Inflammation, Aβ

Author contributions

R.P., C.C., G.S., E.T., S.M. and A.A. conducted experiments and analyzed data. R.P., and A.S. designed experiments and wrote the manuscript. All authors edited the manuscript. A.S. supervised all research.

Declaration of interests

The authors declare no competing interests.

Figure legends

Figure 1: SH3RF3 KD does not affect APP processing but does reduce pTau S422. (A-B) qPCR analysis of SH3RF3 and APP in hPSC-derived neurons treated with non-targeting control or SH3RF3 siRNA. SH3RF3 is significantly knocked down but subsequent effects on APP are only a trend. Data is presented as mean ±SEM with N=3 biological replicates (independent treated wells) for two independent experiments. Comparisons are made with Student's t-test. (C-D) Multiplex ELISA for Aβ from conditioned media (CM) collected from neurons

291 treated with either SH3RF3 or control siRNA. Total Aβ (Aβ42+ Aβ40) levels for are similar for each condition.
292 (C), as is Aβ42/Aβ40 ratio (D). Data is presented as mean ±SEM with N=2-3 biological replicates per experiment
293 for three independent experiments (N=8). Comparisons are made with Student's t-test. (E-F) Western blot
294 analysis of neurons treated with siSH3RF3 or control siRNA subjected to okadaic acid (OKA) or vehicle for 3h.
295 Representative blots and quantification is shown. JNK signaling is strongly activated by OKA as measured by
296 pJNK/JNK ratio (E), which is significantly reduced by SH3R3 KD. Data is presented as mean±SEM with N=2-3
297 biological replicates per experiment for three independent experiments (N=8), Comparison of control Si with
298 OKA and SH3RF3 Si with OKA by ordinary one-way ANOVA, ****<0.0001, *<0.05. pTau S422 phosphorylation
299 (relatively to total tau) is strongly induced by OKA treatment (F), which is decreased by SH3RF3 KD. Data is
300 presented as mean±SEM with N=2 or 3 biological replicates per experiment from 3 independent experiments
301 (N=7-8). Conditions without OKA have undetectable bands for pTau S422 and only conditions with OKA are
302 quantified by comparison of control Si with OKA and SH3RF3 Si with OKA by unpaired t-test, **<0.01.

303 **Figure 2: SH3RF3 knockdown reduces inflammatory cytokine production in iMGLs treated with poly(I:C)**
304 **via modulation of JNK and NFκB pathways.** (A-D**)** iMGLs treated with either siSH3RF3 or control siRNA were
305 subjected to poly(I:C) or vehicle for 2h. qPCR analysis of SH3RF3 (A), IL1β (B), IL6 (C) and TNFα (D) showed
306 successful knockdown of SH3RF3 and induction of all cytokines upon poly(I:C) treatment which were significantly
307 reduced by SH3RF3 KD. Percentage expression was calculated by normalizing gene of interest with respective
308 loading control (GAPDH) for each sample and then all data were normalized to the poly(I:C) treated control
309 siRNA condition and is presented as mean±SEM for N=3 biological replicates per experiment for three
310 independent experiments (N=9). Comparisons between both control Si with poly(I:C) and SH3RF3 Si with
311 poly(I:C) were made with student t test, *<0.5, **<0.01. (E-G) Multiplex ELISA analysis of inflammatory cytokines
312 from conditioned media from iMGLs treated with poly(I:C) for 16h. IL1β (E), IL6 (F) and TNFα (G) all show
313 significant induction by poly(I:C) which is reduced by SH3RF3 KD. Data is presented as mean ±SEM for N=3
314 biological replicates per experiment for three independent experiments (N=9). Statistical comparison among
315 multiple groups were made using one-way ANOVA. (H-I) Western blot analysis of JNK and NFκB pathway
316 activation from iMGLs treated SH3RF3 or control siRNA subjected to poly(I:C) for 6 hr. Representative blots for
317 phosphorylated JNK and total JNK (H), phosphorylated p65 and total p65 (I) with densitometry quantification for
318 3 independent experiments. GAPDH is used as loading control. Data is presented as mean ±SEM for N=3
319 biological replicates per experiment for three independent experiments (N=9). Statistical comparison among
320 multiple groups were made using one-way ANOVA. (J-L) qPCR analysis of IL1β (J), IL6 (K) and TNFα (L) in
321 iMGLs treated with poly(I:C) for 2 hr, with the presence or absence of pathway inhibitors, all of which reduce
322 transcription of all 3 cytokines. CEP-1347 is a JNK pathway (MLK/MAP3K) inhibitor, IKK16 is a NFκB pathway
323 inhibitor, and NSC23766 is a Rac1 inhibitor. Data is presented as mean ±SEM for N=3 biological replicates per
324 experiment for three independent experiments (N=9). Statistical comparison among multiple groups were made
325 using one-way ANOVA. *<0.5, **<0.01, ***<0.001, ****<0.0001
326

Figure 3: SH3RF3 knockdown reduces inflammatory cytokines in iMGLs treated with oAβ42. (A-B) Recombinant monomeric Aβ42 was oligomerized overnight and used for experiments the following day. 200ng of oligomers were run on a 4-20% bis-tris gel and stained with Coomassie blue (A) or transferred onto nitrocellulose membrane (B) to probe against amyloid-β (6E10 antibody). The majority of oligomers have a size consistent with trimers, although higher order species are also present. (C-E) qPCR analysis of inflammatory cytokines IL1β (C), IL6 (D) and TNFα (E) in iMGLs treated with siSH3RF3 or control siRNA subjected to 5 μM oAβ42 or vehicle for 24h. Inflammatory cytokines were statistically reduced by SH3RF3 KD, data is presented as mean±SEM for N=3 biological replicates per experiment for three independent experiments (N=9). Statistical comparison among multiple groups were made using one-way ANOVA. (F-H) Multiplex ELISA analysis of inflammatory cytokines IL1β (F), IL6 (G) and TNFα (H) from conditioned media from iMGLs treated with SH3RF3 or control siRNA subjected to 5 μM oAβ42 for 3 hr. TNFα is statically reduced by SH3RF3 KD. Data is presented as mean ±SEM for N=3 biological replicates per experiment for three independent experiments (N=9). Statistical comparison among multiple groups were made using one-way ANOVA. **<0.01, ***<0.001, ****<0.0001.

Figure 4: SH3RF3 KD reduces JNK and NFkB pathway activation induced by oAβ42 treatment in iMGLs, which is sufficient to reduce inflammatory cytokine production. (A-B) Representative immunoblots and densitometry analysis of JNK (pJNK/JNK, A) and NFkB (phosho-p65/p65, B) pathway activation in iMGLs treated with siSH3RF3 or control siRNA subjected to oAβ42 or vehicle for 3h. Densitometry data is presented as mean ±SEM for N=3 biological per experiment for three independent experiments (N=9). Statistical comparison among multiple groups were made using one-way ANOVA. (C-E) qPCR analysis of inflammatory cytokines IL1β (C), IL6 (D) and TNFα (E) upon 5 μM oAβ42 treatment for 12h in iMGLs pre-treated with either DMSO vehicle, CEP-1347 (JNKi), or IKK16 (NFkBi**)**. Data is presented as mean ±SEM for N=3 per experiment for two independent experiments (N=6). Statistical comparison among multiple groups was made using one-way ANOVA. (F-H) qPCR analysis of inflammatory cytokines IL1β (F), IL6 (G) and TNFα (H) upon 5 μM oAβ42 treatment or vehicle for 6h in isogenic control and PSEN1^{G206A} iMGLs. Data is presented as mean ±SEM for N=3 biological replicates per experiment for three independent experiments (N=9). Statistical comparison among multiple groups were made using one-way ANOVA. **<0.01, ***<0.001, ****<0.0001.

Figure 5: Model of SH3RF3's role in microglial inflammatory responses. SH3RF3 promotes JNK and NFκB signaling in response to oAβ42 or the viral mimic poly(I:C) which in turn transcriptionally upregulates inflammatory cytokines such as IL1β, IL6, and TNFα. Protective SNPs which lower SH3RF3 expression or siRNA-mediated knockdown mimicking these SNPs blunt this response.

Methods

Chart of All Reagents

Reagent or Resource	Source	Identifier

Antibodies		
p-SAPK/JNK (T138/Y185) (81E11)	Cell Signalling Technologies	cat.# 4668S; RRID: AB_823588
SAPK-JNK	Cell Signalling Technologies	cat.# 9252S; RRID: AB_2250373
p-NF-kappaβ P105 (S932)(18E6)	Cell Signalling Technologies	cat.# 4806S; RRID: AB_2282911
NF-kappaβ P105/P50 (SD10D11)	Cell Signalling Technologies	cat.# 13681S
p-c-JUN (S73) (D47G9)	Cell Signalling Technologies	cat.# 3270S; RRID: AB_2895041
c-JUN (L70B11)	Cell Signalling Technologies	cat.# 2315S
CD45 Alexa fluor 647 conjugated	Biolegend	cat.# 304056; RRID: AB_2564155
CD11b Alexa fluor 488 conjugated	Biolegend	cat.# 301318; RRID: AB_493017
IBA1	FUJIFILM	cat. # 019-19741
P2RY12	Millipore-Sigma	cat.# HPA014518; RRID: AB_2669027
TREM2	Cell Signalling Technologies	cat.# 91068S; RRID: AB_2721119
Anti-Aβ 6E10	BioLegend	cat.# SIG-39320; RRID: AB_2715854
Phospho-APP (Thr668)	Cell Signalling Technologies	cat.#6986; RRID:AB_10831197
APP (Y188)	Abcam	cat.# ab_32136; RRID_2289606
Phospho-Tau (Thr217)	Abcam	cat.#ab_192665;RRID_2139718
Phospho-Tau (ser422)	Thermofisher	Cat.#44-764G; RRID_AB_2533748
Total Tau	Dako	Cat.# A0024;RRID_AB_10013724
GAPDH	Thermofisher	cat.# MA1-16757; RRID: AB_568547
Chemicals, peptides, and recombinant proteins		
IL34	R&D	cat.# 5265-IL-010/CF
TGFβ	R&D	cat.# 240-B-010/CF
m-CSF	R&D	cat.# 216-MC-010/CF
CD200	Bon-Opus Bio	cat.# BP004
CX3CL1	R&D	cat.# 365-FR/CF
CEP1347	Tocris	cat.# 4924
IKK16	Tocris	cat.# 2539
NSC23766 (RAC1 inhibitor)	EMD Millipore	cat.# 553502
Amyloid-β-1-42	rPeptide	cat.# A-1163-2
Poly(I:C)	Tocris	cat.# 4287
STEMdiff Hematopoietic Kit	STEMCELL Technologies	cat.# 05310
DMEM-F12 medium	Thermo Fisher	cat.# 11320033
Non-essential amino acids	Thermo Fisher	cat.# 11140050
Insulin-transferrin-selenium	Thermo Fisher	cat.# 41400045
Insulin	Sigma-Aldrich	cat.# 12585014
Glutamax	Thermo Fisher	cat.# 35050061
B27- supplements	Thermo Fisher	cat.# 17504044
N2- supplements	Thermo Fisher	cat.# 17502048

1-Thioglycerol	Sigma-Aldrich	cat.# M-6145
Pen Strep	Thermo Fisher	cat.# 15140122
SuperSignal West Pico PLUS	Thermo Fisher	cat.# 34577
Critical commercial assays and kits		
Aβ peptide panel 1 ELISA kit	Mesoscale Discovery	cat. # K15200E
U-Plex biomarker group 1 (human) ELISA kit	Mesoscale Discovery	cat. # K15067L
Genomic cleavage assay kit	GeneArt, ThermoFisher	cat. #A24372
RNeasy Plus Micro Kit	Qiagen	cat.# 74034
BCA Protein Assay Kit	Millipore Sigma	cat.# 71285-3
Experimental models: Cell lines		
H9 hESC	WiCell	WA09 NIH registry
IMR90 cl.4 iPSC	WiCell	
FA0000010 (FA10) hiPSC	RUCDR	
HEK293	ATCC	
Plasmids		
pMLM3636	Addgene	cat.# 43860, RRID:Addgene_43860
eSpCas9(1.1)	Addgene	cat.# 71814, RRID:Addgene_71814)

362 **Primers**

qPCR	
Human qPCR primers IL1β	F- ATGCACCTGTACGATCACTG
	R- ACAAAGGACATGGAGAACACC
Human qPCR primers IL6	F-CAACCTGAACCTTCCAAAGAT
	R-ACCTCAAACTCCAAAAGACCAG
Human qPCR primers TNFα	F-ACTTTGGAGTGATCGGCC
	R- GCTTGAGGGTTTGCTACAAC
Human qPCR primers SH3RF3	F- AGGACAAAGACCAAGACAAGG
	R- GAGTCATTGAGCTCCACGTAC
Human qPCR primers GAPDH	F- TGAAGGTCGGAGTCAACGGATTTGG
	R-CATGTAGGCCATGAGGTCCACCAC
Dharmacon Accell Pooled siRNA sequences	
Non-targeting	UGGUUUACAUGUCGACUAA
	UGGUUUACAUGUUUUCUGA
	UGGUUUACAUGUUUUCCUA

	UGGUUUACAUGUUGUGUGA
SH3RF3	CCGGAAUAAUGUAGUCGGA
	GAUGCAAACUAGACGAGAA
	CUUUAUGAUUUCGAGAUGA
	CCACUGGCCAAAGGGAUAA
PSEN1 G206A KI	
HDR sequence	GAAGTGTTTAAAACCTATAACGTTGCTGTGGACTACATTACTGTTGCACTCCTGATCTGGAATT TTGcTGTGGTGGGAATGATaTCgATTCACTGGAAAGGTCCACTTCGACTCCAGCAGGCATATC
PSEN1 sgRNA sequence	TTCACTGGAAAGGTCCACTT

hPSC maintenance and differentiation into neurons and microglia-like cells (iMGLs): The FA0000010 (FA10) hiPSC line was acquired from RUCDR, and the IMR90 (cl.4) hiPSC line[72] and the H9 (WA09) hESC line from WiCell. All cultures were grown in the presence of penicillin/streptomycin unless noted otherwise (ThermoFisher) Undifferentiated hPSCs were maintained in StemFlex media (ThermoFisher,) on reduced growth factor Cultrex BME (Biotechne,), and routinely split 1-2 times a week with ReLeSR (STEMCELL Technologies) without ROCKi (Y-27632, Selleck Chemicals) as described previously.[29] Generation and transdifferentiation of permanent transgene hPSCs(Ngn2/rtTA) into exciatory neurons was described in detail previously.[29] In brief, undifferentiated H9 hPSCs with permanent Ngn2/rtTA transgenes (via puromycin selection) were plated in presence of 10 μM Y-27632 (Rocki) on PEI/Laminin-coated surfaces at 55,000-60,000 cells/cm^2 (200k/well of a 12 well) in N2/B27 medium supplemented with 1 μg/mL doxycycline (Sigma-Aldrich), 10 ng/mL BDNF (R&D systems), 10 ng/mL NT3 (R&D systems), and 2 uM AraC (cytarabine, Tocris) which was added for first 7 days of differentiation as needed to deplete non-neuronal cells from culture. At day 7, cultures were switched to Brainphys (N2/SM1) neuronal differentiation medium (STEMCELLTechnologies) supplemented with 1 μg/mL doxycycline, 10 ng/mL BDNF, 10 ng/mL NT3 with half medium change every other day for the duration of differentiation. Brainphys neuronal differentiation medium was further supplemented with 10% mouse astrocyte conditioned media (ACM; ScienCell) from d14 until samples are collected on d28.

hiPSCs were differentiated into iMGLs as described previously with minor adaptations.[52,73] hiPSCs were differentiated into hematopoietic precursors cells (HPCs) using the STEMdiff Hematopoietic kit (STEMCELL Technologies) largely as per manufacturer's instructions. In brief, on day -1 iPSCs were detached with ReLeSR and passaged to achieve a density of 1–2 aggregates/cm^2 of 100-150 cells. Multiple densities were plated in parallel. On day 0, colonies of appropriate density were switched to Medium A from the STEMdiff Hematopoietic Kit to initiate HPC differentiation. On day 3, cells were switched to Medium B with a full media change and fed again with a full media changed on day 5. Cells remained in Medium B for the rest of the HPC differentiation

386 period with Medium B overlay feeds every other day. HPCs were collected 3 independent times by gently
387 removing the floating population with a serological pipette at days 11, 13 and 15 (or days 12, 14 and 16). HPCs
388 were either cryobanked in 45% Medium B, 45% knockout serum replacement (ThermoFisher) and 10% DMSO
389 and stored in liquid nitrogen or directly plated for iMGL induction. Pilot differentiations showed a majority of HPCs
390 were $CD43^+$ as measured by flow cytometry (>90%). HPCs were terminally differentiated by plating 35,000-
391 60,000 cells/cm^2 HPCs on reduced growth factor Cultrex BME in microglia medium (DMEM/F12, 2X insulin-
392 transferrin-selenite, 2X B27, 0.5X N2, 1X glutamax, 1X non-essential amino acids, 400 mM monothioglycerol,
393 and 5 mg/mL human insulin (ThermoFisher) freshly supplemented with 100 ng/mL IL-34, 25 ng/mL M-CSF (R&D
394 Systems) and 50 ng/mL TGFβ1 (STEMCELL Technologies) for every other day until day 24. For the majority of
395 differentiations, differentiating cells were "split" by taking remaining non-adherent cells and plating on to a fresh
396 Cultrex-coated well of the same format (1:1). On day 25, 100 ng/mL CD200 (Bon Opus Biosciences) and
397 100 ng/mL CX3CL1 (R&D Systems) were added to microglia medium to mimic a brain-like environment. For all
398 experiments in this study, iMGLs were treated between day 28 to 35 (post HPC) and samples were collected on
399 days 34-36. The majority of iMGL experiments were generated from FA10 hiPSCs unless stated otherwise.

400 **SH3RF3 knockdown in neurons and iMGLs**: SH3RF3 knockdown was performed using Accell SMARTpool
401 siRNAs targeting SH3RF3, with Accell human non-targeting pool siRNA used as a negative control
402 (Dharmacon/Horizon Discovery). siRNAs were resuspended and delivered as per manufacturer's instructions.
403 In brief, 50 nmol siRNA was resuspended using 1X siRNA buffer at 100 uM stock concentration and directly
404 delivered at 1 uM concentration in cell culture media (at day 21 for neurons, day 28 for iMGLs). Knockdown was
405 performed for 7-days with media overlay ay day 3 and 5. RNA, protein lysates, and conditioned media were
406 collected from neurons at day 28 and iMGLs at day 35.

407 **Treatment of neurons and iMGLs with chemical inhibitors and inflammatory stimuli**: On day 28 neurons
408 were treated with okadaic acid or vehicle for 3 hours before lysing for protein and conditioned media. In some
409 experiments, iMGLs were pre-treated with chemical inhibitors or DMSO vehicle for 2 hr before inflammatory
410 stimuli, which included CEP-1347 (100 nM; Tocris), IKK16 (1 uM; Tocris), and NSC23766 (50 uM; EMD
411 Millipore). iMGLs were then treated with either the dsRNA viral mimic poly(I:C) at (25 ug/mL)[74], oligomerized
412 Aβ42 (5 uM; rPeptide), or vehicle control (dH_2O or F12 media respectively). Recombinant Aβ42 was oligomerized
413 as described previously, [75] and validated via Coomassie blue staining and western blot using the 6E10 antibody
414 (1:1000; BioLegend).
415

416 **qPCR:** RNA was extracted using the RNeasy Plus Micro Kit (Qiagen) and resuspended in 30 µl of RNAse-free
417 water. RNA quantity and quality were assessed with a Nanodrop One (ThermoFisher). For qPCR, 100 ng of
418 RNA was transcribed into complementary DNA Maxima First Strand cDNA Synthesis Kit (Thermo Fisher). Gene
419 expression was assessed using FAST SYBR™ Green Master Mix (ThermoFisher) using primer sets for target
420 genes on a QuantStudio 7 Flex system (Applied Biosystems) and Bio-Rad CFX Opus 384. Gene expression for
421 target genes are normalized to GAPDH and fold change are calculated as $\Delta\Delta C_t$.

422

423 **Amyloid-β42 monomerization, oligomerization and characterization:** Amyloid-β42 was monomerized,
424 stored and later oligomerized as previously described.[75,76] In brief, Aβ(1-42) (rPeptide, 1 mg) vial was allowed to
425 equilibrate to room temperature. Peptides were resuspended in ice-cold Hexafluoroisopropanol (Sigma-Aldrich)
426 to achieve 1 mM concentration directly in a vacuum-sealed vial using Hamilton syringe. The suspension was
427 divided into 8 equal aliquots by volume using a Hamilton syringe into low protein binding Eppendorf tubes,
428 incubated at room temperature for 2h and dried on speedvac at 800g. Upon drying monomerized Aβ(1-42) films
429 can be stored at -80° C for months to years in sealed tubes. For generating oligomers, Eppendorf tubes
430 containing Aβ(1-42) peptide films were equilibrated to room temperature, resuspended in DMSO to achieve 5
431 mM concentration and sonicated at 17° C for 10 min for complete resuspension. Oligomerization was induced
432 by adding phenol-red free F12 to achieve final concentration of 100 μM and incubated at 4° C for 24 to 48 hours.
433 Recombinant monomeric amyloid-β-42 was oligomerized overnight and used for experiments the following day.
434 200ng of oligomers were prepared in the absence of reducing reagents and run on a 4-20% bis-tris gel in MES
435 running buffer. Gels were stained with Coomassie blue overnight or transferred onto 0.2um nitrocellulose
436 membrane to probe against amyloid-β (6E10 antibody, BioLegend).

437

438 **Western blotting**: iMGLs or neurons were harvested using RIPA Lysis Buffer (ThermoFisher) supplemented
439 with Halt protease and phosphatase inhibitors single-use cocktail (ThermoFisher) on ice. 10 ug of lysates and
440 1x Laemmli sample buffer/5% BME were boiled at 95 °C for 10 min. SDS-PAGE was performed by loading
441 samples on Bolt 4–12% gradient Bis-Tris gels (ThermoFisher) using Bolt MOPS buffer (ThermoFisher). For
442 western blotting, nitrocellulose membranes were first blocked with Superblock TBS buffer/0.1% Tween 20
443 (ThermoFisher) for 1h, and then incubated overnight at 4 °C with the following primary antibodies diluted in
444 Superblock/0.1% Tween 20: p-JNK (1:1000; Cell Signaling Technologies), total-JNK(1:1000; Cell Signaling
445 Technologies), phospho-p-50/p105 (1:1000; Cell Signaling Technologies), total p50/p105(1:1000; Cell Signaling
446 Technology), phospho-Tau Ser422 (1:1000; Sigma), phospho-Tau Thr217 (1:1000; Abcam) and GAPDH
447 (1:5000; ThermoFisher). After 3 washes with TBS/0.1% Tween 20, membranes were then incubated with the
448 appropriate HRP-conjugated secondary antibody (1:5000; ThermoFisher) for 1h and washed 3 more times with
449 TBS/0.1% Tween 20. Pierce ECL western blotting substrate (ThermoFisher) or super signal west pico plus
450 chemiluminescent substrate (ThermoFisher) was used to develop chemiluminescence and blots were imaged
451 using the Bio-Rad Chemidoc MP system.

452

453 **Multiplex ELISA for Aβ or IL-1β, IL6 and TNFα:** Conditioned media (CM) from neurons or iMGLs were first
454 spun at 1000 rpms for 3 min., and SNF was aliquoted and stored at -80°C. CM was diluted 1:2 in diluent 35 and
455 processed for ELISA as per the manufacturer's instructions. The Aβ peptide panel 1 ELISA kit and custom
456 cytokine kits U-Plex biomarker group 1 (human) ELISA kit were from Mesoscale Discovery (MSD Quickplex
457 SQ120). Analyte concentrations (pg/mL) was calculated as per manufactures instruction.

458

Immunocytochemistry: iMGLs were plated on low growth factor Cultrex-coated 24-well plates, cultured for 35 days and fixed with 4% paraformaldehyde for 20 min on ice. After fixation, cells were blocked with Superblock blocking buffer in PBS/ 0.1% Triton-X for 1 h and then incubated with the following primary antibodies overnight at 4 °C: α-CD11b (1:100; BD Biosciences) and α-Iba1 (1:200; Wako). Next day, cells were washed thrice with PBS/0.1% Triton-X and then incubated with corresponding Alexa Fluor-conjugated secondary antibodies (1:500; ThermoFisher) at room temperature for 1h. Cells were washed thrice with PBS/0.1% Triton-X and imaged using an ECHO revolve 2 microscope. DAPI (ThermoFisher) was used as a nuclear stain.

PSEN1^{G206A} knock-in via CRISPR/Cas9: The G206A mutation was knocked into both alleles of PSEN1 in IMR90 cl.4 iPSCs using CRISPR/Cas9 as has been done previously for the APP^{Lon} mutation.[77] In brief, sgRNAs targeting exon 7 of PSEN1 were designed (Deskgen.com) and subcloned into MLM3636 vector, a gift from Keith Joung (Addgene plasmid # 43860; http://n2t.net/addgene:43860; RRID:Addgene_43860). sgRNAs were tested for efficacy in HEK293 (ATCC) using a genomic cleavage kit (GeneArt, ThermoFisher). The best sgRNA was used for editing and had the sequence: TTCACTGGAAAGGTCCACTT. The ssDNA HDR template was designed with a silent CRISPR blocking mutation at the PAM site which added a de novo EcoR V restriction site in addition to the G206A mutation. Introduced changes are shown below in bolded under case in the HDR sequence. All oligos were for genome editing were ordered from Integrated DNA technologies. HDR: mutant sequence: GAAGTGTTTAAAACCTATAACGTTGCTGTGGACTACATTACTGTTGCACTCCTGATCTGGAATTT TG**c**TGTGGTGGGAATGAT**a**TC**g**ATTCACTGGAAAGGTCCACTTCGACTCCAGCAGGCATATC, eSpCas9(1.1), a gift from Feng Zhang[78] (Addgene plasmid # 71814 ; http://n2t.net/addgene:71814 ; RRID:Addgene_71814), ssDNA HDR template, sgRNA and GFP plasmid (Lonza) were electroporated (Lonza nucleofector) into feeder-free iPSCs, followed by cell sorting on GFP signal and plating at low density on MEFs (MTI-GlobalStem). Individual clones were manually picked and transferred to 96-well format plate, which was split into duplicate plates and high and low density. gDNA was collected from high density plates as previously described.[79] For each clone, exon 7 of PSEN1 was amplified and screened by restriction digest by EcoR V (New England Biolabs). Sanger sequencing was used to confirm the mutation (Azenta), and successful clones were expanded and banked. PSEN1 G206A knock-in lines were analyzed and demonstrated to have a normal karyotype (Cell Line Genetics) and to be bona fide homozygous knoc-kins rather hemizygous by a quantitative genotyping PCR method.[63] Cl.95 was used in the present study.

Statistics: All experiments were repeated independently and information about number of repeated experiments, replicates, error bars, sample size the statistical test used, and measure of significance are provided in corresponding figure legends. Statistical analyses were performed in Prism software version 9.0 (Graphpad). Unpaired t-test for comparing the means of two groups and one-way ANOVA for comparing means of more than two groups followed by Bonferroni's post-hoc test were used.

496 ## References

497 1. Selkoe, D.J., and Hardy, J. (2016). The amyloid hypothesis of Alzheimer's disease at 25 years. EMBO Mol
498 Med *8*, 595-608. 10.15252/emmm.201606210.
499 2. van Dyck, C.H., Swanson, C.J., Aisen, P., Bateman, R.J., Chen, C., Gee, M., Kanekiyo, M., Li, D., Reyderman,
500 L., Cohen, S., et al. (2023). Lecanemab in Early Alzheimer's Disease. N Engl J Med *388*, 9-21.
501 10.1056/NEJMoa2212948.
502 3. Soderberg, L., Johannesson, M., Nygren, P., Laudon, H., Eriksson, F., Osswald, G., Moller, C., and Lannfelt,
503 L. (2023). Lecanemab, Aducanumab, and Gantenerumab - Binding Profiles to Different Forms of Amyloid-
504 Beta Might Explain Efficacy and Side Effects in Clinical Trials for Alzheimer's Disease. Neurotherapeutics
505 *20*, 195-206. 10.1007/s13311-022-01308-6.
506 4. Lee, J.H., Cheng, R., Vardarajan, B., Lantigua, R., Reyes-Dumeyer, D., Ortmann, W., Graham, R.R.,
507 Bhangale, T., Behrens, T.W., Medrano, M., et al. (2015). Genetic Modifiers of Age at Onset in Carriers of
508 the G206A Mutation in PSEN1 With Familial Alzheimer Disease Among Caribbean Hispanics. JAMA
509 Neurol *72*, 1043-1051. 10.1001/jamaneurol.2015.1424.
510 5. Park, Y.P., and Kellis, M. (2021). CoCoA-diff: counterfactual inference for single-cell gene expression
511 analysis. Genome Biol *22*, 228. 10.1186/s13059-021-02438-4.
512 6. Jia, P., Zhao, Z., Hulgan, T., Bush, W.S., Samuels, D.C., Bloss, C.S., Heaton, R.K., Ellis, R.J., Schork, N., Marra,
513 C.M., et al. (2017). Genome-wide association study of HIV-associated neurocognitive disorder (HAND):
514 A CHARTER group study. Am J Med Genet B Neuropsychiatr Genet *174*, 413-426. 10.1002/ajmg.b.32530.
515 7. Karkkainen, S., van der Linden, M., and Renkema, G.H. (2010). POSH2 is a RING finger E3 ligase with Rac1
516 binding activity through a partial CRIB domain. FEBS Lett *584*, 3867-3872. 10.1016/j.febslet.2010.07.060.
517 8. Tapon, N., Nagata, K., Lamarche, N., and Hall, A. (1998). A new rac target POSH is an SH3-containing
518 scaffold protein involved in the JNK and NF-kappaB signalling pathways. EMBO J *17*, 1395-1404.
519 10.1093/emboj/17.5.1395.
520 9. Zhang, P., Liu, Y., Lian, C., Cao, X., Wang, Y., Li, X., Cong, M., Tian, P., Zhang, X., Wei, G., et al. (2020).
521 SH3RF3 promotes breast cancer stem-like properties via JNK activation and PTX3 upregulation. Nat
522 Commun *11*, 2487. 10.1038/s41467-020-16051-9.
523 10. Xu, Z., Kukekov, N.V., and Greene, L.A. (2003). POSH acts as a scaffold for a multiprotein complex that
524 mediates JNK activation in apoptosis. EMBO J *22*, 252-261. 10.1093/emboj/cdg021.
525 11. Kukekov, N.V., Xu, Z., and Greene, L.A. (2006). Direct interaction of the molecular scaffolds POSH and JIP
526 is required for apoptotic activation of JNKs. J Biol Chem *281*, 15517-15524. 10.1074/jbc.M601056200.
527 12. Wilhelm, M., Kukekov, N.V., Schmit, T.L., Biagas, K.V., Sproul, A.A., Gire, S., Maes, M.E., Xu, Z., and
528 Greene, L.A. (2012). Sh3rf2/POSHER protein promotes cell survival by ring-mediated proteasomal
529 degradation of the c-Jun N-terminal kinase scaffold POSH (Plenty of SH3s) protein. J Biol Chem *287*, 2247-
530 2256. 10.1074/jbc.M111.269431.
531 13. Kim, E.K., and Choi, E.J. (2010). Pathological roles of MAPK signaling pathways in human diseases.
532 Biochim Biophys Acta *1802*, 396-405. 10.1016/j.bbadis.2009.12.009.
533 14. Yarza, R., Vela, S., Solas, M., and Ramirez, M.J. (2015). c-Jun N-terminal Kinase (JNK) Signaling as a
534 Therapeutic Target for Alzheimer's Disease. Front Pharmacol *6*, 321. 10.3389/fphar.2015.00321.
535 15. Sun, E., Motolani, A., Campos, L., and Lu, T. (2022). The Pivotal Role of NF-kB in the Pathogenesis and
536 Therapeutics of Alzheimer's Disease. Int J Mol Sci *23*. 10.3390/ijms23168972.
537 16. Shi, Z.M., Han, Y.W., Han, X.H., Zhang, K., Chang, Y.N., Hu, Z.M., Qi, H.X., Ting, C., Zhen, Z., and Hong, W.
538 (2016). Upstream regulators and downstream effectors of NF-kappaB in Alzheimer's disease. J Neurol
539 Sci *366*, 127-134. 10.1016/j.jns.2016.05.022.
540 17. Lee, M.S., Kao, S.C., Lemere, C.A., Xia, W., Tseng, H.C., Zhou, Y., Neve, R., Ahlijanian, M.K., and Tsai, L.H.
541 (2003). APP processing is regulated by cytoplasmic phosphorylation. J Cell Biol *163*, 83-95.
542 10.1083/jcb.200301115.

18. Colombo, A., Bastone, A., Ploia, C., Sclip, A., Salmona, M., Forloni, G., and Borsello, T. (2009). JNK regulates APP cleavage and degradation in a model of Alzheimer's disease. Neurobiol Dis *33*, 518-525. 10.1016/j.nbd.2008.12.014.
19. Yoon, S.O., Park, D.J., Ryu, J.C., Ozer, H.G., Tep, C., Shin, Y.J., Lim, T.H., Pastorino, L., Kunwar, A.J., Walton, J.C., et al. (2012). JNK3 perpetuates metabolic stress induced by Abeta peptides. Neuron *75*, 824-837. 10.1016/j.neuron.2012.06.024.
20. Yoshida, H., Hastie, C.J., McLauchlan, H., Cohen, P., and Goedert, M. (2004). Phosphorylation of microtubule-associated protein tau by isoforms of c-Jun N-terminal kinase (JNK). J Neurochem *90*, 352-358. 10.1111/j.1471-4159.2004.02479.x.
21. Reynolds, C.H., Utton, M.A., Gibb, G.M., Yates, A., and Anderton, B.H. (1997). Stress-activated protein kinase/c-jun N-terminal kinase phosphorylates tau protein. J Neurochem *68*, 1736-1744. 10.1046/j.1471-4159.1997.68041736.x.
22. Tamagno, E., Guglielmotto, M., Giliberto, L., Vitali, A., Borghi, R., Autelli, R., Danni, O., and Tabaton, M. (2009). JNK and ERK1/2 pathways have a dual opposite effect on the expression of BACE1. Neurobiol Aging *30*, 1563-1573. 10.1016/j.neurobiolaging.2007.12.015.
23. Troy, C.M., Rabacchi, S.A., Xu, Z., Maroney, A.C., Connors, T.J., Shelanski, M.L., and Greene, L.A. (2001). beta-Amyloid-induced neuronal apoptosis requires c-Jun N-terminal kinase activation. J Neurochem *77*, 157-164. 10.1046/j.1471-4159.2001.t01-1-00218.x.
24. Dong, W., Embury, C.M., Lu, Y., Whitmire, S.M., Dyavarshetty, B., Gelbard, H.A., Gendelman, H.E., and Kiyota, T. (2016). The mixed-lineage kinase 3 inhibitor URMC-099 facilitates microglial amyloid-beta degradation. J Neuroinflammation *13*, 184. 10.1186/s12974-016-0646-z.
25. Zhong, L., Zhang, Z.L., Li, X., Liao, C., Mou, P., Wang, T., Wang, Z., Wang, Z., Wei, M., Xu, H., et al. (2017). TREM2/DAP12 Complex Regulates Inflammatory Responses in Microglia via the JNK Signaling Pathway. Front Aging Neurosci *9*, 204. 10.3389/fnagi.2017.00204.
26. Ruganzu, J.B., Peng, X., He, Y., Wu, X., Zheng, Q., Ding, B., Lin, C., Guo, H., Yang, Z., Zhang, X., and Yang, W. (2022). Downregulation of TREM2 expression exacerbates neuroinflammatory responses through TLR4-mediated MAPK signaling pathway in a transgenic mouse model of Alzheimer's disease. Mol Immunol *142*, 22-36. 10.1016/j.molimm.2021.12.018.
27. Chen, C.H., Zhou, W., Liu, S., Deng, Y., Cai, F., Tone, M., Tone, Y., Tong, Y., and Song, W. (2012). Increased NF-kappaB signalling up-regulates BACE1 expression and its therapeutic potential in Alzheimer's disease. Int J Neuropsychopharmacol *15*, 77-90. 10.1017/S1461145711000149.
28. Mancuso, R., Fattorelli, N., Martinez-Muriana, A., Davis, E., Wolfs, L., Van Den Daele, J., Geric, I., Premereur, J., Polanco, P., Bijnens, B., et al. (2024). Xenografted human microglia display diverse transcriptomic states in response to Alzheimer's disease-related amyloid-beta pathology. Nat Neurosci *27*, 886-900. 10.1038/s41593-024-01600-y.
29. Song, S., Ashok, A., Williams, D., Kaufman, M., Duff, K., and Sproul, A. (2021). Efficient Derivation of Excitatory and Inhibitory Neurons from Human Pluripotent Stem Cells Stably Expressing Direct Reprogramming Factors. Curr Protoc *1*, e141. 10.1002/cpz1.141.
30. Huang, Y.A., Zhou, B., Wernig, M., and Sudhof, T.C. (2017). ApoE2, ApoE3, and ApoE4 Differentially Stimulate APP Transcription and Abeta Secretion. Cell *168*, 427-441 e421. 10.1016/j.cell.2016.12.044.
31. Vogel, J., Anand, V.S., Ludwig, B., Nawoschik, S., Dunlop, J., and Braithwaite, S.P. (2009). The JNK pathway amplifies and drives subcellular changes in tau phosphorylation. Neuropharmacology *57*, 539-550. 10.1016/j.neuropharm.2009.07.021.
32. Kim, D., Su, J., and Cotman, C.W. (1999). Sequence of neurodegeneration and accumulation of phosphorylated tau in cultured neurons after okadaic acid treatment. Brain Res *839*, 253-262. 10.1016/s0006-8993(99)01724-2.

589 33. Hasegawa, M., Jakes, R., Crowther, R.A., Lee, V.M., Ihara, Y., and Goedert, M. (1996). Characterization of
590 mAb AP422, a novel phosphorylation-dependent monoclonal antibody against tau protein. FEBS Lett
591 *384*, 25-30. 10.1016/0014-5793(96)00271-2.
592 34. Deters, N., Ittner, L.M., and Gotz, J. (2008). Divergent phosphorylation pattern of tau in P301L tau
593 transgenic mice. Eur J Neurosci *28*, 137-147. 10.1111/j.1460-9568.2008.06318.x.
594 35. Haase, C., Stieler, J.T., Arendt, T., and Holzer, M. (2004). Pseudophosphorylation of tau protein alters its
595 ability for self-aggregation. J Neurochem *88*, 1509-1520. 10.1046/j.1471-4159.2003.02287.x.
596 36. Montoliu-Gaya, L., Benedet, A.L., Tissot, C., Vrillon, A., Ashton, N.J., Brum, W.S., Lantero-Rodriguez, J.,
597 Stevenson, J., Nilsson, J., Sauer, M., et al. (2023). Mass spectrometric simultaneous quantification of tau
598 species in plasma shows differential associations with amyloid and tau pathologies. Nat Aging *3*, 661-
599 669. 10.1038/s43587-023-00405-1.
600 37. Barthelemy, N.R., Mallipeddi, N., Moiseyev, P., Sato, C., and Bateman, R.J. (2019). Tau Phosphorylation
601 Rates Measured by Mass Spectrometry Differ in the Intracellular Brain vs. Extracellular Cerebrospinal
602 Fluid Compartments and Are Differentially Affected by Alzheimer's Disease. Front Aging Neurosci *11*,
603 121. 10.3389/fnagi.2019.00121.
604 38. Merighi, S., Nigro, M., Travagli, A., and Gessi, S. (2022). Microglia and Alzheimer's Disease. Int J Mol Sci
605 *23*. 10.3390/ijms232112990.
606 39. Mehan, S., Meena, H., Sharma, D., and Sankhla, R. (2011). JNK: a stress-activated protein kinase
607 therapeutic strategies and involvement in Alzheimer's and various neurodegenerative abnormalities. J
608 Mol Neurosci *43*, 376-390. 10.1007/s12031-010-9454-6.
609 40. Zhang, Y., Sloan, S.A., Clarke, L.E., Caneda, C., Plaza, C.A., Blumenthal, P.D., Vogel, H., Steinberg, G.K.,
610 Edwards, M.S., Li, G., et al. (2016). Purification and Characterization of Progenitor and Mature Human
611 Astrocytes Reveals Transcriptional and Functional Differences with Mouse. Neuron *89*, 37-53.
612 10.1016/j.neuron.2015.11.013.
613 41. Zhang, Y., Chen, K., Sloan, S.A., Bennett, M.L., Scholze, A.R., O'Keeffe, S., Phatnani, H.P., Guarnieri, P.,
614 Caneda, C., Ruderisch, N., et al. (2014). An RNA-sequencing transcriptome and splicing database of glia,
615 neurons, and vascular cells of the cerebral cortex. J Neurosci *34*, 11929-11947.
616 10.1523/JNEUROSCI.1860-14.2014.
617 42. Levine, K.S., Leonard, H.L., Blauwendraat, C., Iwaki, H., Johnson, N., Bandres-Ciga, S., Ferrucci, L., Faghri,
618 F., Singleton, A.B., and Nalls, M.A. (2023). Virus exposure and neurodegenerative disease risk across
619 national biobanks. Neuron *111*, 1086-1093 e1082. 10.1016/j.neuron.2022.12.029.
620 43. Steel, A.J., and Eslick, G.D. (2015). Herpes Viruses Increase the Risk of Alzheimer's Disease: A Meta-
621 Analysis. J Alzheimers Dis *47*, 351-364. 10.3233/JAD-140822.
622 44. Liu, N., Jiang, X., and Li, H. (2023). The viral hypothesis in Alzheimer's disease: SARS-CoV-2 on the cusp.
623 Front Aging Neurosci *15*, 1129640. 10.3389/fnagi.2023.1129640.
624 45. Priemer, D.S., Rhodes, C.H., Karlovich, E., Perl, D.P., and Goldman, J.E. (2022). Abeta Deposits in the
625 Neocortex of Adult and Infant Hypoxic Brains, Including in Cases of COVID-19. J Neuropathol Exp Neurol
626 *81*, 988-995. 10.1093/jnen/nlac095.
627 46. Shen, W.B., Elahi, M., Logue, J., Yang, P., Baracco, L., Reece, E.A., Wang, B., Li, L., Blanchard, T.G., Han,
628 Z., et al. (2022). SARS-CoV-2 invades cognitive centers of the brain and induces Alzheimer's-like
629 neuropathology. bioRxiv. 10.1101/2022.01.31.478476.
630 47. Kumar, V. (2019). Toll-like receptors in the pathogenesis of neuroinflammation. J Neuroimmunol *332*,
631 16-30. 10.1016/j.jneuroim.2019.03.012.
632 48. Wang, W.Y., Tan, M.S., Yu, J.T., and Tan, L. (2015). Role of pro-inflammatory cytokines released from
633 microglia in Alzheimer's disease. Ann Transl Med *3*, 136. 10.3978/j.issn.2305-5839.2015.03.49.
634 49. <Oligodendrocytes damage in Alzheimer's disease Beta amyloid toxicity and inflammation.pdf>.

50. Cai, Y., Liu, J., Wang, B., Sun, M., and Yang, H. (2022). Microglia in the Neuroinflammatory Pathogenesis of Alzheimer's Disease and Related Therapeutic Targets. Front Immunol *13*, 856376. 10.3389/fimmu.2022.856376.
51. He, Y., Taylor, N., Yao, X., and Bhattacharya, A. (2021). Mouse primary microglia respond differently to LPS and poly(I:C) in vitro. Sci Rep *11*, 10447. 10.1038/s41598-021-89777-1.
52. McQuade, A., Coburn, M., Tu, C.H., Hasselmann, J., Davtyan, H., and Blurton-Jones, M. (2018). Development and validation of a simplified method to generate human microglia from pluripotent stem cells. Mol Neurodegener *13*, 67. 10.1186/s13024-018-0297-x.
53. Maroney, A.C., Finn, J.P., Connors, T.J., Durkin, J.T., Angeles, T., Gessner, G., Xu, Z., Meyer, S.L., Savage, M.J., Greene, L.A., et al. (2001). Cep-1347 (KT7515), a semisynthetic inhibitor of the mixed lineage kinase family. J Biol Chem *276*, 25302-25308. 10.1074/jbc.M011601200.
54. Parkinson Study Group, P.I. (2007). Mixed lineage kinase inhibitor CEP-1347 fails to delay disability in early Parkinson disease. Neurology *69*, 1480-1490. 10.1212/01.wnl.0000277648.63931.c0.
55. Waelchli, R., Bollbuck, B., Bruns, C., Buhl, T., Eder, J., Feifel, R., Hersperger, R., Janser, P., Revesz, L., Zerwes, H.G., and Schlapbach, A. (2006). Design and preparation of 2-benzamido-pyrimidines as inhibitors of IKK. Bioorg Med Chem Lett *16*, 108-112. 10.1016/j.bmcl.2005.09.035.
56. Zhang, Q.G., Wang, R., Han, D., Dong, Y., and Brann, D.W. (2009). Role of Rac1 GTPase in JNK signaling and delayed neuronal cell death following global cerebral ischemia. Brain Res *1265*, 138-147. 10.1016/j.brainres.2009.01.033.
57. <Discovery and characterization of small molecule Rac1 inhibitors.pdf>.
58. Dhawan, G., Floden, A.M., and Combs, C.K. (2012). Amyloid-beta oligomers stimulate microglia through a tyrosine kinase dependent mechanism. Neurobiol Aging *33*, 2247-2261. 10.1016/j.neurobiolaging.2011.10.027.
59. Parajuli, B., Sonobe, Y., Horiuchi, H., Takeuchi, H., Mizuno, T., and Suzumura, A. (2013). Oligomeric amyloid beta induces IL-1beta processing via production of ROS: implication in Alzheimer's disease. Cell Death Dis *4*, e975. 10.1038/cddis.2013.503.
60. Fa, M., Orozco, I.J., Francis, Y.I., Saeed, F., Gong, Y., and Arancio, O. (2010). Preparation of oligomeric beta-amyloid 1-42 and induction of synaptic plasticity impairment on hippocampal slices. J Vis Exp. 10.3791/1884.
61. Quiroga, I.Y., Cruikshank, A.E., Bond, M.L., Reed, K.S.M., Evangelista, B.A., Tseng, J.H., Ragusa, J.V., Meeker, R.B., Won, H., Cohen, S., et al. (2022). Synthetic amyloid beta does not induce a robust transcriptional response in innate immune cell culture systems. J Neuroinflammation *19*, 99. 10.1186/s12974-022-02459-1.
62. Konttinen, H., Cabral-da-Silva, M.E.C., Ohtonen, S., Wojciechowski, S., Shakirzyanova, A., Caligola, S., Giugno, R., Ishchenko, Y., Hernandez, D., Fazaludeen, M.F., et al. (2019). PSEN1DeltaE9, APPswe, and APOE4 Confer Disparate Phenotypes in Human iPSC-Derived Microglia. Stem Cell Reports *13*, 669-683. 10.1016/j.stemcr.2019.08.004.
63. Weisheit, I., Kroeger, J.A., Malik, R., Klimmt, J., Crusius, D., Dannert, A., Dichgans, M., and Paquet, D. (2020). Detection of Deleterious On-Target Effects after HDR-Mediated CRISPR Editing. Cell Rep *31*, 107689. 10.1016/j.celrep.2020.107689.
64. Ma, Q.L., Yang, F., Rosario, E.R., Ubeda, O.J., Beech, W., Gant, D.J., Chen, P.P., Hudspeth, B., Chen, C., Zhao, Y., et al. (2009). Beta-amyloid oligomers induce phosphorylation of tau and inactivation of insulin receptor substrate via c-Jun N-terminal kinase signaling: suppression by omega-3 fatty acids and curcumin. J Neurosci *29*, 9078-9089. 10.1523/JNEUROSCI.1071-09.2009.
65. Guillozet-Bongaarts, A.L., Cahill, M.E., Cryns, V.L., Reynolds, M.R., Berry, R.W., and Binder, L.I. (2006). Pseudophosphorylation of tau at serine 422 inhibits caspase cleavage: in vitro evidence and implications for tangle formation in vivo. J Neurochem *97*, 1005-1014. 10.1111/j.1471-4159.2006.03784.x.

682 66. Salminen, A., Kauppinen, A., and Kaarniranta, K. (2017). Hypoxia/ischemia activate processing of Amyloid
683 Precursor Protein: impact of vascular dysfunction in the pathogenesis of Alzheimer's disease. J
684 Neurochem *140*, 536-549. 10.1111/jnc.13932.
685 67. Lund, S., Porzgen, P., Mortensen, A.L., Hasseldam, H., Bozyczko-Coyne, D., Morath, S., Hartung, T.,
686 Bianchi, M., Ghezzi, P., Bsibsi, M., et al. (2005). Inhibition of microglial inflammation by the MLK inhibitor
687 CEP-1347. J Neurochem *92*, 1439-1451. 10.1111/j.1471-4159.2005.03014.x.
688 68. Kiyota, T., Machhi, J., Lu, Y., Dyavarshetty, B., Nemati, M., Zhang, G., Mosley, R.L., Gelbard, H.A., and
689 Gendelman, H.E. (2018). URMC-099 facilitates amyloid-beta clearance in a murine model of Alzheimer's
690 disease. J Neuroinflammation *15*, 137. 10.1186/s12974-018-1172-y.
691 69. Maroney, A.C., Finn, J.P., Bozyczko-Coyne, D., O'Kane, T.M., Neff, N.T., Tolkovsky, A.M., Park, D.S., Yan,
692 C.Y., Troy, C.M., and Greene, L.A. (1999). CEP-1347 (KT7515), an inhibitor of JNK activation, rescues
693 sympathetic neurons and neuronally differentiated PC12 cells from death evoked by three distinct
694 insults. J Neurochem *73*, 1901-1912.
695 70. Waldmeier, P., Bozyczko-Coyne, D., Williams, M., and Vaught, J.L. (2006). Recent clinical failures in
696 Parkinson's disease with apoptosis inhibitors underline the need for a paradigm shift in drug discovery
697 for neurodegenerative diseases. Biochem Pharmacol *72*, 1197-1206. 10.1016/j.bcp.2006.06.031.
698 71. Chen, X., Rzhetskaya, M., Kareva, T., Bland, R., During, M.J., Tank, A.W., Kholodilov, N., and Burke, R.E.
699 (2008). Antiapoptotic and trophic effects of dominant-negative forms of dual leucine zipper kinase in
700 dopamine neurons of the substantia nigra in vivo. J Neurosci *28*, 672-680. 10.1523/JNEUROSCI.2132-
701 07.2008.
702 72. Yu, J., Vodyanik, M.A., Smuga-Otto, K., Antosiewicz-Bourget, J., Frane, J.L., Tian, S., Nie, J., Jonsdottir,
703 G.A., Ruotti, V., Stewart, R., et al. (2007). Induced pluripotent stem cell lines derived from human somatic
704 cells. Science *318*, 1917-1920. 10.1126/science.1151526.
705 73. Abud, E.M., Ramirez, R.N., Martinez, E.S., Healy, L.M., Nguyen, C.H.H., Newman, S.A., Yeromin, A.V.,
706 Scarfone, V.M., Marsh, S.E., Fimbres, C., et al. (2017). iPSC-Derived Human Microglia-like Cells to Study
707 Neurological Diseases. Neuron *94*, 278-293 e279. 10.1016/j.neuron.2017.03.042.
708 74. Lafaille, F.G., Pessach, I.M., Zhang, S.Y., Ciancanelli, M.J., Herman, M., Abhyankar, A., Ying, S.W., Keros,
709 S., Goldstein, P.A., Mostoslavsky, G., et al. (2012). Impaired intrinsic immunity to HSV-1 in human iPSC-
710 derived TLR3-deficient CNS cells. Nature *491*, 769-773. 10.1038/nature11583.
711 75. Kim, Y.A., Siddiqui, T., Blaze, J., Cosacak, M.I., Winters, T., Kumar, A., Tein, E., Sproul, A.A., Teich, A.F.,
712 Bartolini, F., et al. (2023). RNA methyltransferase NSun2 deficiency promotes neurodegeneration
713 through epitranscriptomic regulation of tau phosphorylation. Acta Neuropathol *145*, 29-48.
714 10.1007/s00401-022-02511-7.
715 76. Stine, W.B., Jr., Dahlgren, K.N., Krafft, G.A., and LaDu, M.J. (2003). In vitro characterization of conditions
716 for amyloid-beta peptide oligomerization and fibrillogenesis. J Biol Chem *278*, 11612-11622.
717 10.1074/jbc.M210207200.
718 77. Sun, J., Carlson-Stevermer, J., Das, U., Shen, M., Delenclos, M., Snead, A.M., Koo, S.Y., Wang, L., Qiao, D.,
719 Loi, J., et al. (2019). CRISPR/Cas9 editing of APP C-terminus attenuates beta-cleavage and promotes
720 alpha-cleavage. Nat Commun *10*, 53. 10.1038/s41467-018-07971-8.
721 78. Slaymaker, I.M., Gao, L., Zetsche, B., Scott, D.A., Yan, W.X., and Zhang, F. (2016). Rationally engineered
722 Cas9 nucleases with improved specificity. Science *351*, 84-88. 10.1126/science.aad5227.
723 79. Paquet, D., Kwart, D., Chen, A., Sproul, A., Jacob, S., Teo, S., Olsen, K.M., Gregg, A., Noggle, S., and Tessier-
724 Lavigne, M. (2016). Efficient introduction of specific homozygous and heterozygous mutations using
725 CRISPR/Cas9. Nature *533*, 125-129. 10.1038/nature17664.
726

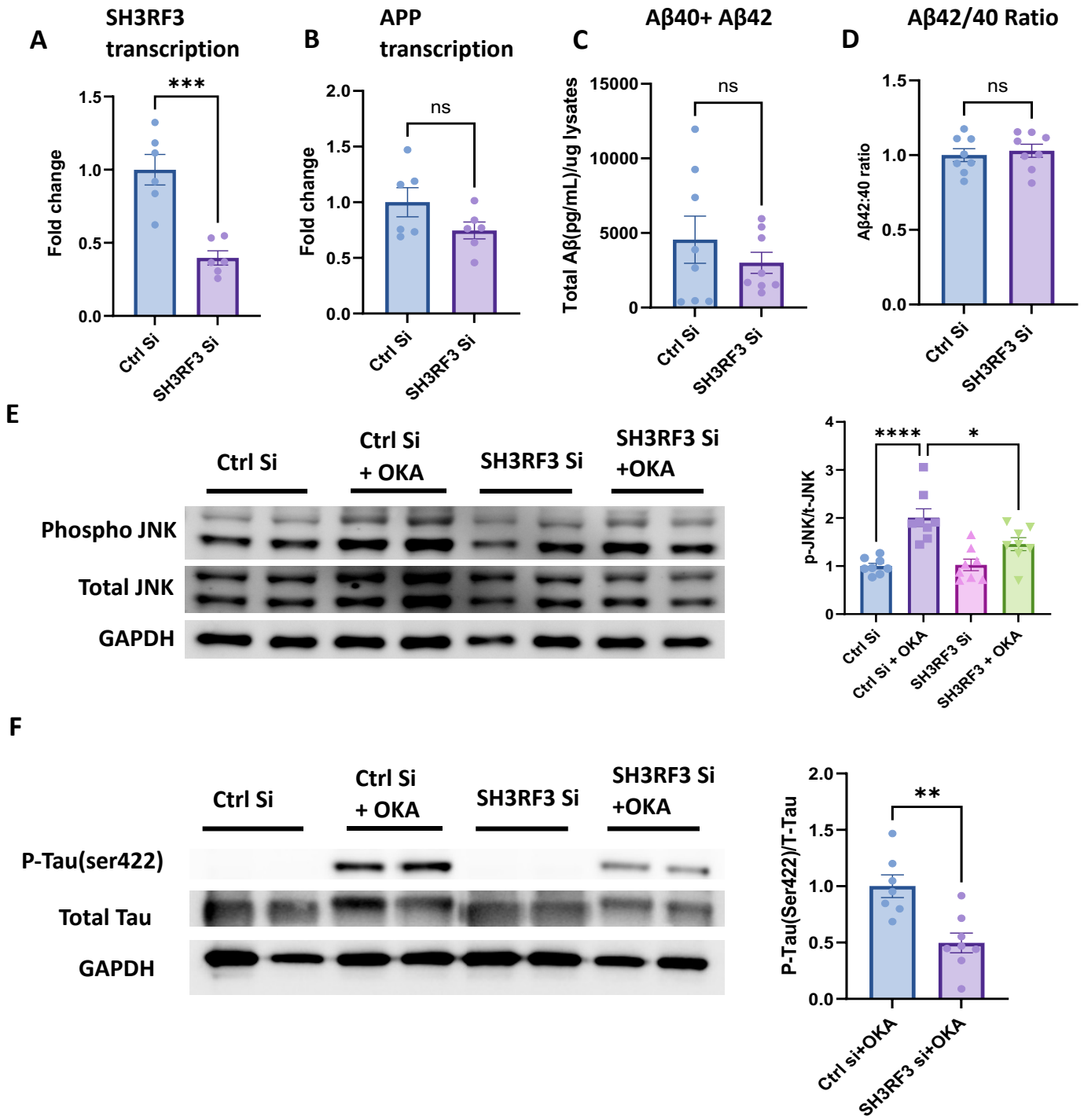
A
SH3RF3 transcription
***
Fold change
1.5
1.0
0.5
0.0
Ctrl Si
SH3RF3 Si
B
APP transcription
ns
Fold change
2.0
1.5
1.0
0.5
0.0
Ctrl Si
SH3RF3 Si
C
Aβ40+ Aβ42
ns
Total Aβ(pg/mL)/ug lysates
15000
10000
5000
0
Ctrl Si
SH3RF3 Si
D
Aβ42/40 Ratio
ns
Aβ42:40 ratio
1.5
1.0
0.5
0.0
Ctrl Si
SH3RF3 Si
E
Ctrl Si
Ctrl Si + OKA
SH3RF3 Si
SH3RF3 Si +OKA
Phospho JNK
Total JNK
GAPDH
****
*
p-JNK/t-JNK
4
3
2
1
0
Ctrl Si
Ctrl Si + OKA
SH3RF3 Si
SH3RF3 + OKA
F
Ctrl Si
Ctrl Si + OKA
SH3RF3 Si
SH3RF3 Si +OKA
P-Tau(ser422)
Total Tau
GAPDH
**
P-Tau(Ser422)/T-Tau
2.0
1.5
1.0
0.5
0.0
Ctrl si+OKA
SH3RF3 si+OKA

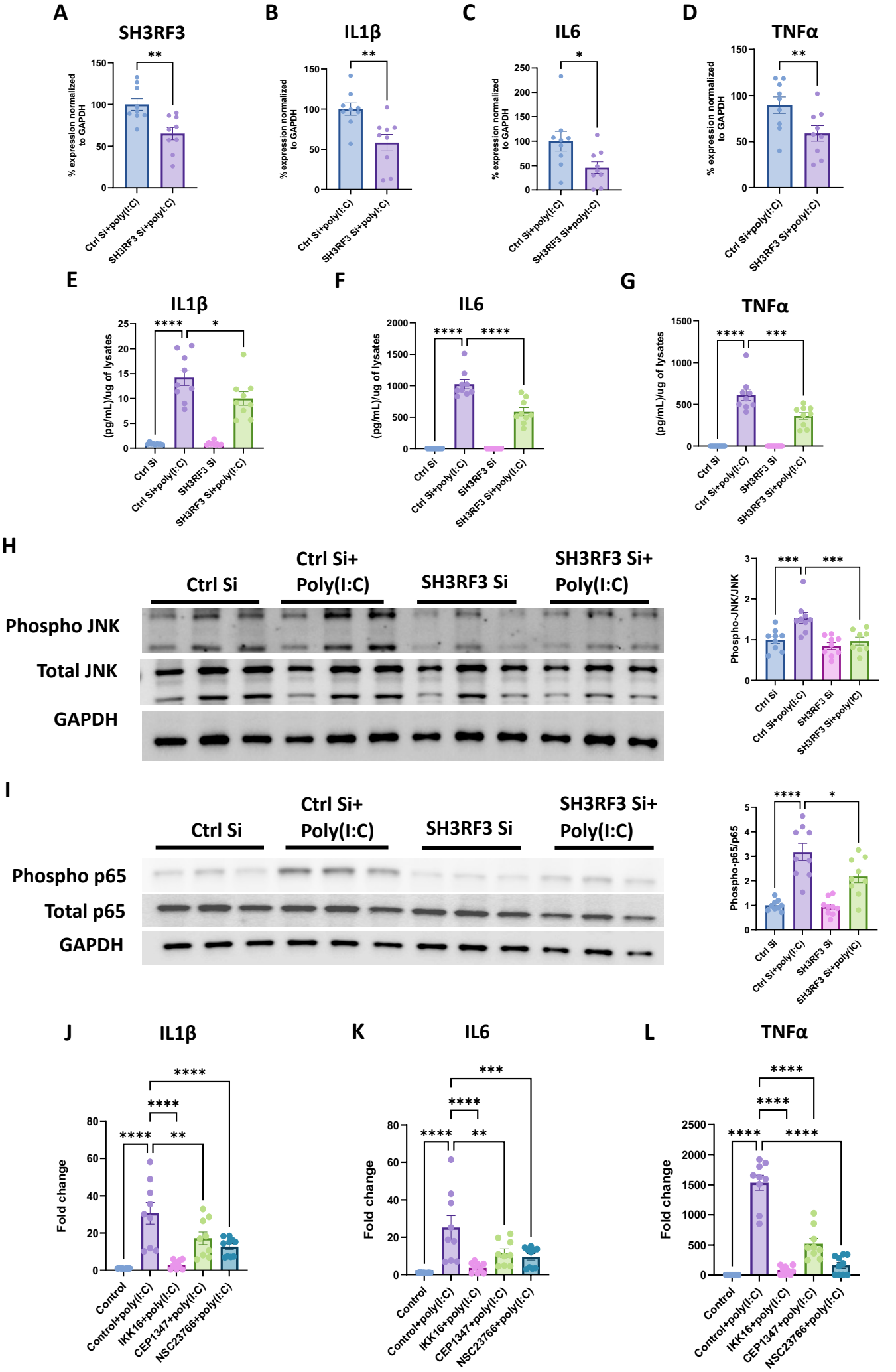
A
SH3RF3
% expression normalized to GAPDH
Ctrl Si+poly(I:C)
SH3RF3 Si+poly(I:C)
B
IL1β
C
IL6
D
TNFα
E
IL1β
(pg/mL)/ug of lysates
Ctrl Si
Ctrl Si+poly(I:C)
SH3RF3 Si
SH3RF3 Si+poly(I:C)
F
IL6
G
TNFα
H
Ctrl Si
Ctrl Si+ Poly(I:C)
SH3RF3 Si
SH3RF3 Si+ Poly(I:C)
Phospho JNK
Total JNK
GAPDH
Phospho-JNK/JNK
I
Phospho p65
Total p65
GAPDH
Phospho-p65/p65
J
IL1β
Fold change
Control
Control+poly(I:C)
IKK16+poly(I:C)
CEP1347+poly(I:C)
NSC23766+poly(I:C)
K
IL6
L
TNFα

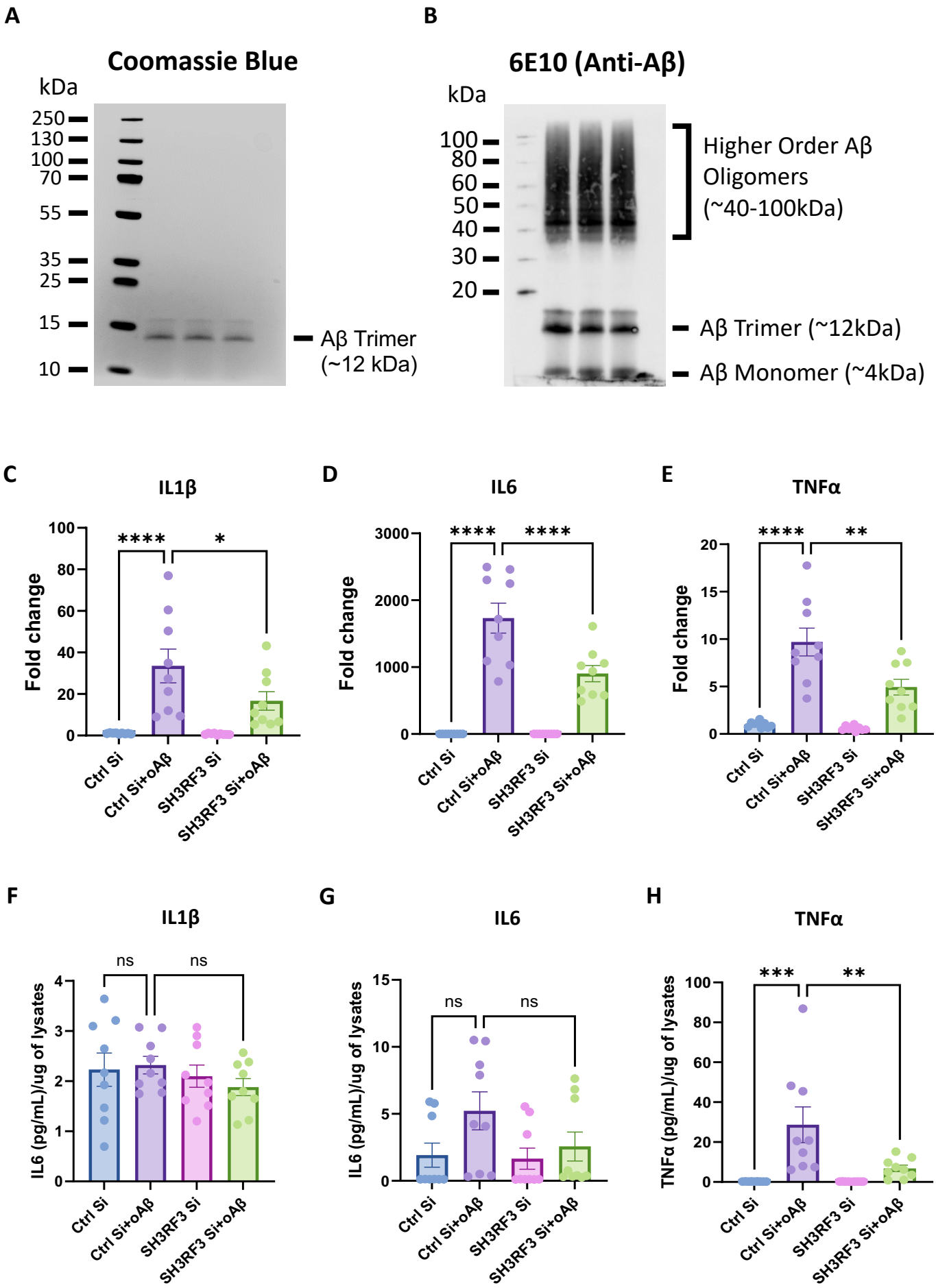
A
Coomassie Blue
kDa
250
130
100
70
55
35
25
15
10
Aβ Trimer
(~12 kDa)
B
6E10 (Anti-Aβ)
kDa
100
80
60
50
40
30
20
Higher Order Aβ
Oligomers
(~40-100kDa)
Aβ Trimer (~12kDa)
Aβ Monomer (~4kDa)
C
IL1β
Fold change
****
*
D
IL6
Fold change
****
****
E
TNFα
Fold change
****
**
Ctrl Si
Ctrl Si+oAβ
SH3RF3 Si
SH3RF3 Si+oAβ
F
IL1β
IL6 (pg/mL)/ug of lysates
ns
ns
G
IL6
IL6 (pg/mL)/ug of lysates
ns
ns
H
TNFα
TNFα (pg/mL)/ug of lysates
***
**

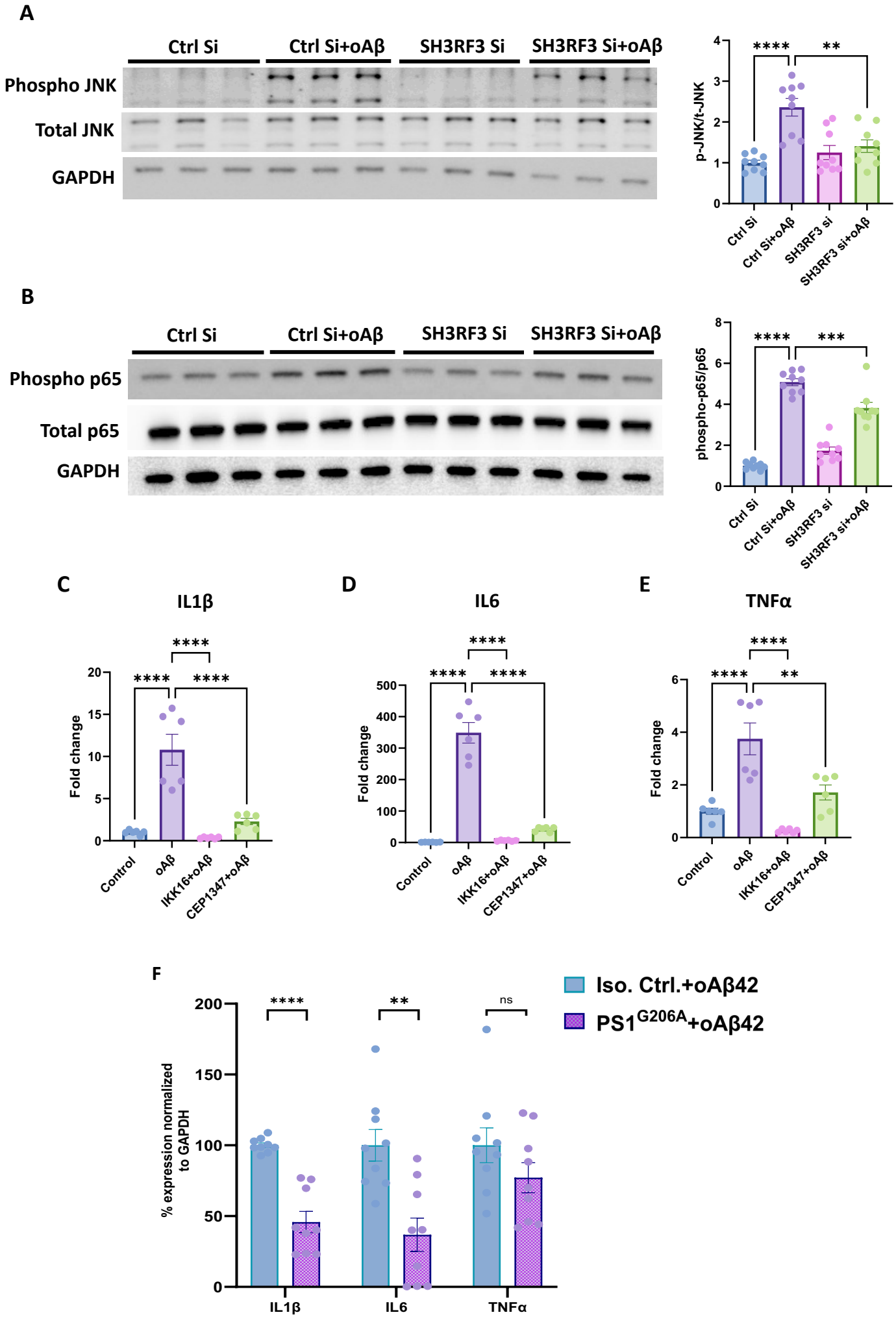
A
Ctrl Si
Ctrl Si+oAβ
SH3RF3 Si
SH3RF3 Si+oAβ
Phospho JNK
Total JNK
GAPDH
p-JNK/t-JNK
****
**
Ctrl Si
Ctrl Si+oAβ
SH3RF3 si
SH3RF3 si+oAβ
B
Ctrl Si
Ctrl Si+oAβ
SH3RF3 Si
SH3RF3 Si+oAβ
Phospho p65
Total p65
GAPDH
phospho-p65/p65
****
***
Ctrl Si
Ctrl Si+oAβ
SH3RF3 si
SH3RF3 si+oAβ
C
IL1β
Fold change
****
****
****
Control
oAβ
IKK16+oAβ
CEP1347+oAβ
D
IL6
Fold change
****
****
****
Control
oAβ
IKK16+oAβ
CEP1347+oAβ
E
TNFα
Fold change
****
****
**
Control
oAβ
IKK16+oAβ
CEP1347+oAβ
F
Iso. Ctrl.+oAβ42
PS1G206A+oAβ42
% expression normalized to GAPDH
****
**
ns
IL1β
IL6
TNFα

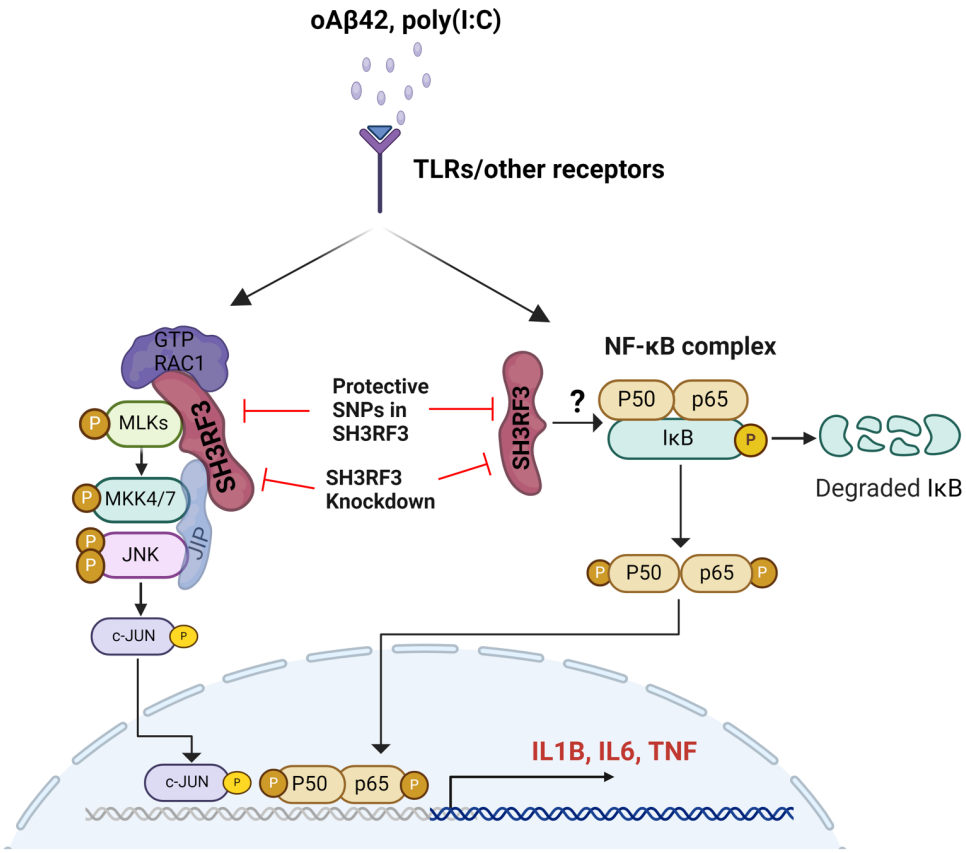
oAβ42, poly(I:C)
TLRs/other receptors
GTP
RAC1
MLKs
MKK4/7
JNK
SH3RF3
JIP
c-JUN
Protective
SNPs in
SH3RF3
SH3RF3
Knockdown
SH3RF3
?
NF-κB complex
P50
p65
IκB
Degraded IκB
P50
p65
c-JUN
P50
p65
IL1B, IL6, TNF